Effects of Graft Length and Density of Well-Defined Graft Polymers on the Thermoresponsive Behavior and Self-Assembly Morphology

Bingyan Jiang,[1,2] Lei Zhang,[1,2] Jie Yan,[1,2] Qingquan Huang,[1,2] Bing Liao,[1] Hao Pang[1]

[1]Guangzhou Institute of Chemistry, Chinese Academy of Sciences, Guangzhou 510650, China
[2]Guangzhou Institute of Chemistry, University of Chinese Academy of Sciences, Beijing 100049, China
Correspondence to: H. Pang (E-mail: panghao@gic.ac.cn)

Received 7 February 2014; accepted 11 May 2014; published online 2 June 2014
DOI: 10.1002/pola.27256

ABSTRACT: A series of well-defined thermoresponsive graft polymers with different lengths and graft densities, poly(glycidyl methacrylate)-*graft*-poly(*N*-isopropylacrylate) (PGMA-*g*-PNIPAM), were successfully prepared by combination of controlled/living free radical polymerization and click chemistry. Effects of grafting length and density on the thermoresponsive behavior, aggregating mean diameter, and self-assembly morphology are systematically investigated. The thermosensitive characteristics of graft polymers in aqueous solution prove that the length and graft density had positive co-relationship with the lower critical solution temperature value and mean diameter of micelles as well as the size distribution, while the effect of graft length of polymers is more significant than that of density. Transmission electron microscopy analysis shows that the conformations of $PGMA_{45}$-*g*-$PNIPAM_{20}$ and $PGMA_{45}$-*g*-$PNIPAM_{46}$ with longer length and bigger grafting density in aqueous solutions are spherical nanoparticles with the increasing trend of the diameters, while that of $PGMA_{45}$-*g*-$PNIPAM_{(73, 50\%)}$ shows a spherical-like morphology, which indicates that the graft length and density have a significant effect on the mean diameter of micelle but not on the self-assembly morphology. These results reveal that to obtain desired thermoresponsive behavior and self-assembly morphology of functional polymers, it is essential to design and fabricate the structure of graft polymers with proper length and graft density. © 2014 Wiley Periodicals, Inc. J. Polym. Sci., Part A: Polym. Chem. **2014**, *52*, 2442–2453

KEYWORDS: atom transfer radical polymerization (ATRP); click chemistry; controllable graft length; graft copolymers; graft density; particle size distribution; reversible addition fragmentation chain transfer (RAFT); self-assembly; stimuli-sensitive polymers; thermoresponsive

INTRODUCTION Graft copolymers with inversed architectures have attracted great interest in recent years owing to their unique physical and chemical properties, solution properties, and broad potential application in science, biochemistry, and industry.[1–5] A variety of these copolymers with complex structures, such as block-graft polymers,[6,7] heterograft macromolecules,[8,9] and star-graft polymers,[10,11] are prepared by combining synthetic strategies, including "graft-from" by grafting monomer from the backbone,[12] "graft-onto" by attaching preformed side chains onto the backbone, and "graft-though" by (co)polymerizing macromolecules.[13,14] It is well known that the graft macromolecular parameters, including chemical composition, molar mass, main-chain topology, length, and graft density of side chains, have a great effect on their properties, especially their solution properties and micellization process.[15–17] Many works lay stress on the synthesis of polymers with complex architectures and emphasize the polymerization process[18–20]; a few systematical reports focus on the investigation of the effect of the graft architecture on the solution properties and micellar morphology of graft polymers.

Compared with block copolymers, graft polymers with well-defined architectures are much more difficult to be prepared owing to their complex architectures and steric repulsion, and the solution properties are more complicated. In particular, it is reported that the rate of the thermal response of graft polymers in aqueous solution is significantly faster than block polymers in some cases, so the thermoresponsive graft polymers are regarded as advanced functional materials in various scientific and industrial fields.[21,22] Poly(*N*-isopropylacrylate) (PNIPAM), as one of the most widely studied thermoresponsive water-soluble homopolymer since 1956, undergoes a coil-globule transition and exhibits phase separation at lower critical solution temperature (LCST) of 32 °C in aqueous solutions, which is close to physiological temperature and also is insensitive to the difference of molecular weight and concentration.[23–25] Given the aforementioned merits of PNIPAM and the advantage of convenient

preparation by rapid development of controlled/living radical polymerization (CLRP), some well-defined smart polymers based on PNIPAM have drawn considerable attention.[26–28] The most versatile and efficient techniques, including atom transfer radical polymerization (ATRP)[29,30] and reversible addition-fragmentation chain transfer (RAFT) polymerization,[31–33] are applied by many researchers to prepare some well-defined thermoresponsive polymers based on PNIPAM.[34–37] To reduce the steric hindrance and the interaction of hydrogen bonds when preparing graft polymers based on PNIPAM with controlled length and high graft density, choosing an efficient and specific method under mild conditions to obtain these polymers is a fascinating subject for chemists. Click chemistry, as a high coupling method, is widely used to prepare some complex macromolecules, even for the preparation of functional graft polymers with high graft density and steric hindrance.[38] At present, the combination of CLRP techniques and click chemistry is regarded as a revolutionary method for the synthesis of many functional graft copolymers with high-yield chemical transformation and unique physical and chemical properties, especially thermoresponsive graft polymers.[39,40]

Glycidyl methacrylate (GMA) is often used to synthesize some novel functional polymers with excellent properties and can supply many active sites for further postmodification. In view of these advantages, many groups use this monomer to prepare some macromolecular brushes with novel structures, especially thermoresponsive materials.[41–44] Meanwhile, there are also a few reports about preparing well-defined thermoresponsive graft copolymers based on PNIPAM with different molecular weights by using GMA as functional monomer. Zhao and coworkers reported the synthesis of an asymmetric macromolecular brush using PGMA as backbone and poly(ethylene glycol) not only as backbone but also as side chain as well as polystyrene and PNIPAM as side chains by ARTP, RAFT, and click method and investigated the morphology of aggregates of micelles and thermoresponsive behavior.[45] They also prepared amphiphilic asymmetric comb polymer with pendant pyrene groups and two kinds of PNIPAM with different molecular weights as side chain by RAFT and click chemistry, and investigated the photophysical properties and self-assembly behaviors of polymer in solution.[46] Cai et al. also reported a series of surface-functionalized graft copolymer membrane with different molecular weight and a fixed graft density (8.85%) of PNIPAM and studied the temperature-dependent flux of microporous membranes.[47] Fu et al. prepared a solvent-resistant thermoresponsive nanofiber and investigated the smart surface of fibers.[48] These reports refer to the complicated graft architectures and the thermoresponsive characteristics based on PNIPAM, while the relationship between the thermoresponsive behaviors of graft polymers and the length as well as the density of the side chains are not investigated in detail. To obtain a deep understanding of this relationship, it has a great significance to prepare a series of well-defined simple thermoresponsive graft copolymers to investigate the architecture and the property relationships by combination of CLRP techniques and click chemistry. However, such studies are rarely found to our best knowledge, especially those focusing on the effect of the graft length and density on the thermoresponsive property and self-assembly morphology.

To investigate the effect of graft length and density on the thermoresponsive characteristic, aggregating properties, and morphology, we prepared a series of well-defined thermoresponsive graft polymers with PGMA as backbone and PNIPAMs as thermoresponsive side chains with different length and graft density by combining ATRP, RAFT, and click chemistry. Our work included: first, the polymer backbone PGMA with pendent epoxy groups was prepared by ATRP and then ring-opened by NaN_3; second, alkynyl-terminated thermoresponsive homopolymers PNIPAM with different degree of polymerization (DP) were synthesized by RAFT; two homopolymers were combined together through click reaction to prepare the target graft polymers. The thermoresponsive properties of all graft polymers in aqueous solutions were investigated using dynamic light scattering (DLS) and ultraviolet–visible (UV–vis) spectroscopy at different temperatures. The aggregation morphologies of the graft polymers with different length and graft density in aqueous solution were measured by transmission electron microscopy (TEM). The results would provide some valuable guidance for investigating the relationship among the graft architecture and the thermoresponsive properties and the micellar morphology, and for designing and fabricating controllable thermosensitive graft polymers.

EXPERIMENTAL

Materials

GMA (Duodian, Nanjing, China) was passed through a column of alumina powder to remove the inhibitor and then purified by vacuum-distilled before storing in refrigerator. *N*-isopropylacrylamide (NIPAM, Aladdin, 97%) was recrystallized in hexane, dimethylaminopyridine (DMAP, Aladdin, 99%) in toluene, and azodiisobutyronitrile (AIBN) in methanol. Ligand *N,N,N′,N′,N″*-pentamethyldiethylenetriamine (PMDETA, Aladdin, 99%), sodium azide, ammonium chloride, propargyl alcohol (PA, Xiya reagents, 99%), 1-(3-dimethylaminopropyl)-3-ethylcarbodiimide hydrochloride (EDC·HCl, Aladdin, 98.5%), ethyl α-bromoisobutyrate (EBB, Aladdin, 98%), and disodium ethylene diamine tetraacetate (EDTA-Na_2, Tianjin Kermel, China) were used as received. Catalysts CuBr and CuCl were purified by washing with glacial acetic acid in 90 °C for 8 h and then washed with acetone and ethyl ether before drying under vacuum. *N*,*N*-Dimethylformamide (DMF) and diphenyl ether (DPE) were dried though CaH_2 for 24 h and then distilled. *S*-1-butyl-*S′*-(α-methyl-α′-acetic acid) trithiocarbonate was synthesized according to previous literature.[49] All other reagents were used without further purification.

Preparation of S-1-Butyl-S′-(α-methyl-α′-propargyl acetate) Trithiocarbonate (CTA)

Alkynyl-terminated trithiocarbonate was synthesized by esterification of *S*-1-butyl-*S′*-(α-methyl-α′-acetic acid)

trithiocarbonate and propargyl alcohol according to ref. 45. *S*-1-butyl-*S*′-(α-methyl-α′-acetic acid) trithiocarbonate (15.5 g, 68.5 mmol), EDC·HCl (19.6 g, 0.1 mol), and DMAP (12.5 g, 0.1 mol) were mixed with 400 mL of dry CH_2Cl_2 and purged with pure argon into flask for 1 h. Propargyl alcohol (12.5 mL, 0.2 mol) was added dropwise to the mixture at 0 °C for 30 min, and the yellow solution was stirred at room temperature for 48 h. Then CH_2Cl_2 was removed by rotary evaporator and the resulting mixture was successfully washed with 3 N HCl, 1 N sodium bicarbonate, and saturated NaCl for five times before drying over anhydrous magnesium sulfate. After purified by silica column chromatography using petroleum ether/ethyl acetate (60/1, v/v) as the eluent, *S*−1-butyl-*S*′-(α-methyl-α′-propargyl acetate) trithiocarbonate was obtained as red oil (yield: 76%).

FTIR (KBr, cm^{-1}): 3300 (HC≡C—), 2130 (C≡C), 1735 (O═CO O—), 1070 (C═S); ^{1}H NMR (400 MHz, $CDCl_3$, δ): 4.72 (s, 2H, —C***H***$_2$—C≡CH), 3.36 (t, 2H, —S—C***H***$_2$—CH_2—), 2.51 (s, 1H, ***H***C≡C—), 4.84 (m, 1H, —OOC—C***H***(CH_3)—), 1.65 (d, 3H, —OOC—CH(C***H***$_3$)—), 1.69 (m, 2H, —C***H***$_2$—CH_2—CH_3), 1.37 (m, 2H, —CH_2—C***H***$_2$—CH_3), 0.85 (t, 3H, —CH_2—CH_2—C***H***$_3$); ^{13}C NMR (400 MHz, $CDCl_3$, δ): 13.7 (***C***H_3—CH_2—), 16.7 (—CH(***C***H_3) —S—), 21.9 (CH_3—***C***H_2—), 30.1 (—***C***H_2—CH_2—), 37.2 (—***C***H_2—S—), 46.9 (—***C***H(CH_3)—S—), 56.4 (—O—***C***H_2—), 67.5 (H***C***≡C—), 84.3 (HC≡***C***—), 172.1 (—O—***C***═O), 221.3 (—S—***C***(═S)—S—). $C_{11}H_{16}O_2S_3$: MS (MH^+, Chem. Ion.): calculated for 276.0191, found for 276.0177.

Preparation of Alkynyl-Poly(N-isopropylacrylamide) (Alkynyl-PNIPAM) by RAFT

The polymer PNIPAM with alkyne as end group was synthesized by RAFT in DMF using alkynyl-terminated trithiocarbonate as a chain transfer agent in the present of initiator AIBN. Alkynyl-PNIPAM was prepared as follows. A mixture of NIPAM (3.5935 g, 31.7 mmol), *S*-1-butyl-*S*′-(α-methyl-α′-propargyl acetate) trithiocarbonate (0.1752 g, 0.634 mmol), and AIBN (0.0108 g, 0.0656 mmol) in 10 mL of dry DMF was put into the round-bottomed flask followed by purging with pure argon for 1 h, then degassed by three freeze–pump–thaw cycles, followed by stirring at 70 °C for a certain time. Samples were withdrawn at different intervals for conversion analysis (^{1}H NMR) and molecular weight (gel permeation chromatography, GPC). When the reaction ended, the mixture was then cooled in liquid nitrogen and then exposed to air. After diluted with THF, the mixture was slowly poured into excess *n*-hexane to produce light yellow solid before vacuum drying at room temperature to a constant weight. On the basis of ^{1}H NMR result, the conversion was about 92.2% by comparing the peak area of 4.62 ppm with the characteristic peak area of 3.96 ppm, and the actual DP of alkynyl-PNIPAM was 46. Thus, the product was denoted as alkynyl-$PNIPAM_{46}$. Other homopolymers alkynyl-PNIPAM with DP of 20 and 73 were synthesized by similar method.

^{1}H NMR (400 MHz, $CDCl_3$, δ, ppm): 1.1 ((—CH(C***H***$_3$)$_3$—)), 3.9 ((—C***H***(CH_3)$_3$—)), 1.0 (C***H***$_3$—CH_2—, —CH(C***H***$_3$)—), 1.4 (CH_3—C***H***$_2$—), 1.68 (—C***H***$_2$—CH_2—S—, —CH—C***H***$_2$—), 2.0 (—C***H***—CH_2—), 3.3 (—CH_2—C***H***$_2$—S—), 4.7 (—C***H***$_2$—OC═O); ^{13}C NMR (400 MHz, $CDCl_3$, δ, ppm): 23.9 (—C(***C***H_3)$_3$—), 31.6 (—CH—***C***H_2—), 41.6 (—***C***(CH_3)$_3$—), 44.3 (—***C***H—CH_2—), 56.8 (—O—***C***H_2—), 67.7 (H***C***≡C—), 84.6 (HC≡***C***—), 179.5 (O═***C***—NH—).

Polymerization of Poly(glycidyl methacrylate) by ATRP

The reaction was performed in a two-flask set connecting two 25-mL flasks via a glass pipe. One flask was added into EBB (0.1006 g, 0.516 mmol), GMA (3.05208 g, 0.0248 mol), and PMDETA (0.1788 g, 1.03 mmol) in 7.5-mL dried DPE, while CuCl (0.0511 g, 0.516 mmol) was loaded to the other flask equipped with a magnetic stirrer. After three freeze–pump–thaw cycles, the liquid mixture was carefully transferred to the other flask containing catalyst CuCl and maintained at 28 °C for 1.5 h. The polymerization was quenched in liquid nitrogen before exposure to air, and then the mixture was diluted with CH_2Cl_2 and passed through a neutral alumina column to remove the copper complex. The filtrate was concentrated with rotary evaporation before precipitating in hexane. The crude product was purified for three times by dissolving in CH_2Cl_2 and precipitating in *n*-hexane, and then dried under vacuum at room temperature for 24 h to give white powder. On the basis of ^{1}H NMR result, the conversion is about 93.8% by comparing with the peak area of the terminal methene group at the peak of 4.1 and the characteristic peak of 3.21 ppm, and the actual DP of PGMA was 45. Thus, the product was denoted as $PGMA_{45}$.

Ring-Opened PGMA by Sodium Azide (PGMA-OH/N_3)

In a typical procedure, PGMA (2.0 g, 14 mmol of epoxide groups) was dissolved in 70 mL of dried DMF. Sodium azide (2.73 g, 42 mmol) and ammonium chloride (2.247 g, 42 mmol) were added into the solution, and the mixture was stirred at 30 °C for 48 h. After removing most DMF, the product was precipitated in cold water and filtrated followed by washing with water for four times, and dried under vacuum at room temperature for 2 days. The yield of the white product was about 85%.

Preparation of PGMA-g-PNIPAM by Click Reaction

The alkyne-containing polymer alkynyl-PNIPAM with different DPs described above was reacted with PGMA-OH/N_3 in the presence of CuBr and PMDETA in DMF by click reaction. To a 25-mL round-bottomed flask equipped with a magnetic stir bar, PGMA-OH/N_3 (0.2 g, 1.08 mol of azide groups), alkynyl-$PNIPAM_{46}$ (2.956 g, 0.54 mmol, about 50 mol % of azide groups), and CuBr (0.0775 g, 0.54 mmol) were dissolved in 5.5 mL of DMF. The flask was sealed with a rubber septum and the air was evacuated by purging with argon for 50 min. The ligand PMDETA (0.1404 g, 0.81 mmol) was quickly added and then backfilled with argon again for 40 min. The mixture was reacted at room temperature for 3 days and then propargyl alcohol was introduced to react with excessive azide groups. The mixture was dialyzed against methanol for 4 days and distilled water for 3 days followed by freeze-dried for 48 h to obtain 2.87 g copolymer (yield: 92%). Other graft polymers with different graft

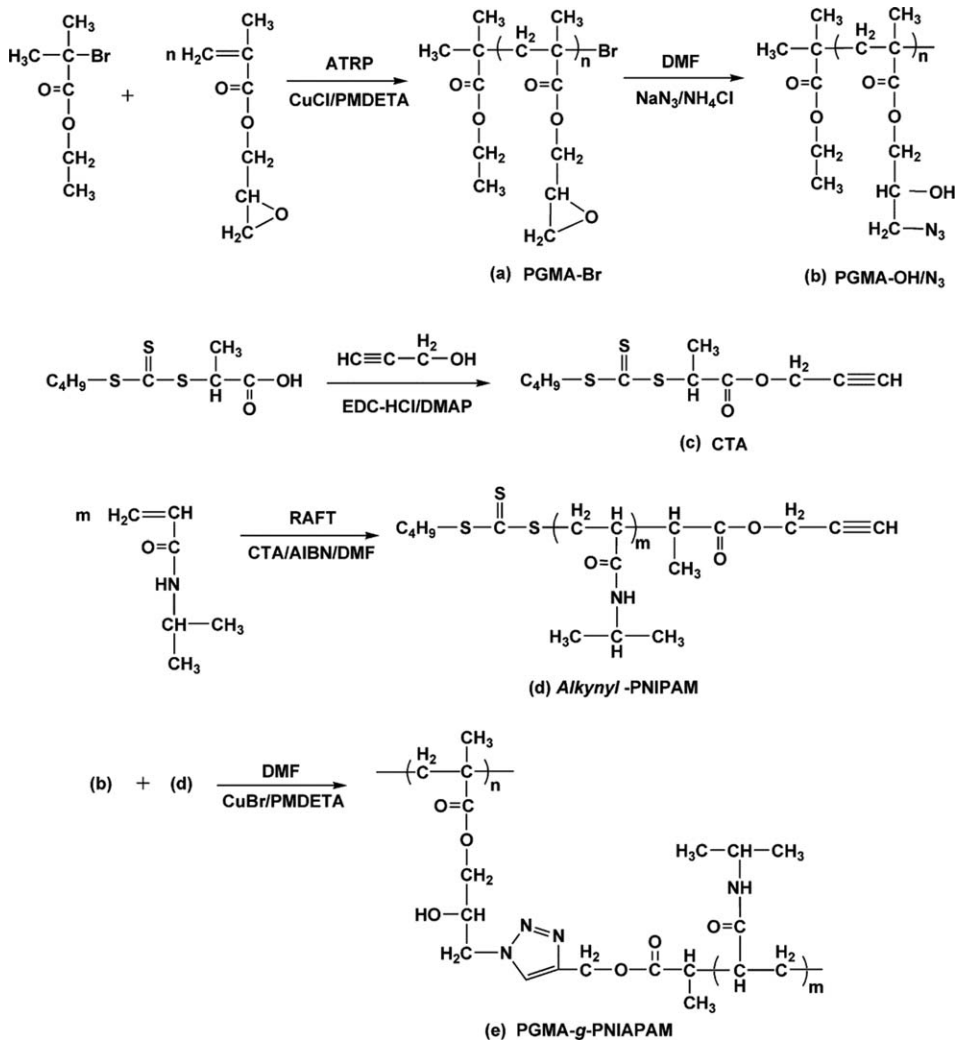

SCHEME 1 The synthetic route for graft polymer PGMA-*g*-PNIPAM.

density and DPs of alkynyl-PNIPAM were also synthesized according to the aforementioned method.

Characterization

All NMR spectra were recorded on a Bruker DMX-400 spectrometer with $CDCl_3$ or deuterated DMSO as solvent and tetramethylsilane as internal reference. EI/MS analyses were carried out using a Shimadzu GCMS-QP5050A mass spectrometer. The apparent molecular weights (M_n) and molecular weight distributions (M_w/M_n) were measured at 35 °C by a GPC with a Waters 1515 series GPC system equipped with a Waters 717 autosampler and a Waters 2414 refractive index (RI) detector as well as a set column of styragel HR4 and HR3. DMF was used as eluent at a flow rate of 1.0 mL/min and polystyrene as the calibration standards. Fourier transform infrared absorption spectra (FTIR) were obtained using Bruker TENSOR 27 (Germany) at a scan range of 500–4000 cm^{-1}. Cloud point temperatures (CPs) of micelles were determined by transmittance measurements in a 3-mL quartz cell on a Hitachi (3010) UV–vis spectrometer equipped with a temperature controller and two-position sample holder. The polymer concentration was 2 mg/mL. The light transmittance of aqueous solutions for the varied polymers was monitored at 500 nm at a heating rate of 1.0 °C/min, and the data were collected after the solution was equilibrated for 30 min. The hydrodynamic diameters of the self-assembly aggregates were measured on a Zetasizer Nano ZS90 from Malvern Instruments equipped with a 10 mW He–Ne laser at a wavelength of 633 nm and with temperature controller, and the results were analyzed by CONTIN mode. TEM images were obtained on a JEM-100CXII equipped with Model 794 CCD camera (512 × 512) at an operating voltage of 200 kV. The TEM specimens were prepared by depositing solution containing 0.15 wt % of polymer on coating 200 meshes Formvar-coated grids and then dried in vacuum desiccators at room temperature. The specimens were stained by phosphotungstic acid (PTA, 1.5 wt % aqueous solution, pH = 7).

RESULTS AND DISCUSSION

Synthetic scheme for preparing thermoresponsive graft polymers PGMA-*g*-PNIPAM is shown in Scheme 1, using CRLP

TABLE 1 Summary of Structural Parameters of PGMA, PGMA-OH/N_3, Alkynyl-PNIPAM, and PGMA-*g*-PNIPAM[a]

Entry	Sample	Click Efficiency (%)	$M_{n,th}$[b] ($\times 10^4$g/mol)	$M_{n,NMR}$[c] ($\times 10^4$g/mol)	$M_{n,GPC}$[d] ($\times 10^4$g/mol)	PDI[d]
1	$PGMA_{45}$-Br	—	0.76	0.66	0.98	1.12
2	$PGMA_{45}$-OH/N_3	—	—	—	1.04	1.31
3	Alkynyl-$PNIPAM_{20}$	—	0.33	0.25	0.23	1.15
4	Alkynyl-$PNIPAM_{46}$	—	0.57	0.55	0.49	1.12
5	Alkynyl-$PNIPAM_{73}$	—	0.98	0.94	0.74	1.14
6	$PGMA_{45}$-*g*-$PNIPAM_{20}$	25	—	—	291.64	1.14
7	$PGMA_{45}$-*g*-$PNIPAM_{20}$	50	—	—	320.51	1.16
8	$PGMA_{45}$-*g*-$PNIPAM_{20}$	75	—	—	349.26	1.16
9	$PGMA_{45}$-*g*-$PNIPAM_{46}$	25	—	—	354.64	1.14
10	$PGMA_{45}$-*g*-$PNIPAM_{46}$	50	—	—	421.77	1.15
11	$PGMA_{45}$-*g*-$PNIPAM_{46}$	75	—	—	470.07	1.12
12	$PGMA_{45}$-*g*-$PNIPAM_{73}$	25	—	—	451.21	1.14
13	$PGMA_{45}$-*g*-$PNIPAM_{73}$	50	—	—	516.11	1.16
14	$PGMA_{45}$-*g*-$PNIPAM_{73}$	75	—	—	603.21	1.26

[a] DP was determined by ^{1}H NMR.
[b] Theoretical molecular weights ($M_{n,th}$) were determined by monomer conversion.
[c] The number-average molecular weights were determined by ^{1}H NMR.
[d] The number-average molecular weight ($M_{n,GPC}$) and the polydispersity index (PDI) were measured by gel permeation chromatograph (GPC) on PS standards.

techniques of ATRP, RAFT, and high-efficiency click reaction. The structural parameters of all the intermediate and final products are summarized in Table 1.

The homopolymer PGMA-Br was prepared in DPE at 30 °C with ethyl α-bromoisobutyrate as initiator and with CuCl/PMDETA as catalyst, and this work also appeared in Zhao's laboratory.[45] The ^{1}H NMR spectrum of homopolymer PGMA-Br is shown in Figure 1(left a). According to the characteristic chemical shifts, it clearly showed the evidence for successful polymerization. The FTIR spectrum of homopolymer PGMA-Br in Figure 1(right a) also confirmed the formation of homopolymer PGMA with the characteristic band at 908 cm^{-1} for epoxy group; no evidence of alkene groups was shown in NMR and FIIR. Meanwhile, the apparent number-average molecular weight and molecular weight distribution of diblock polymer are presented in Figure 2(d); the typical GPC trace of homopolymer revealed that a monomodal and symmetric elution peak was shown in the curve.

After ring-opened the epoxy groups on the side chain in the presence of sodium azide, the structure of this polymer was

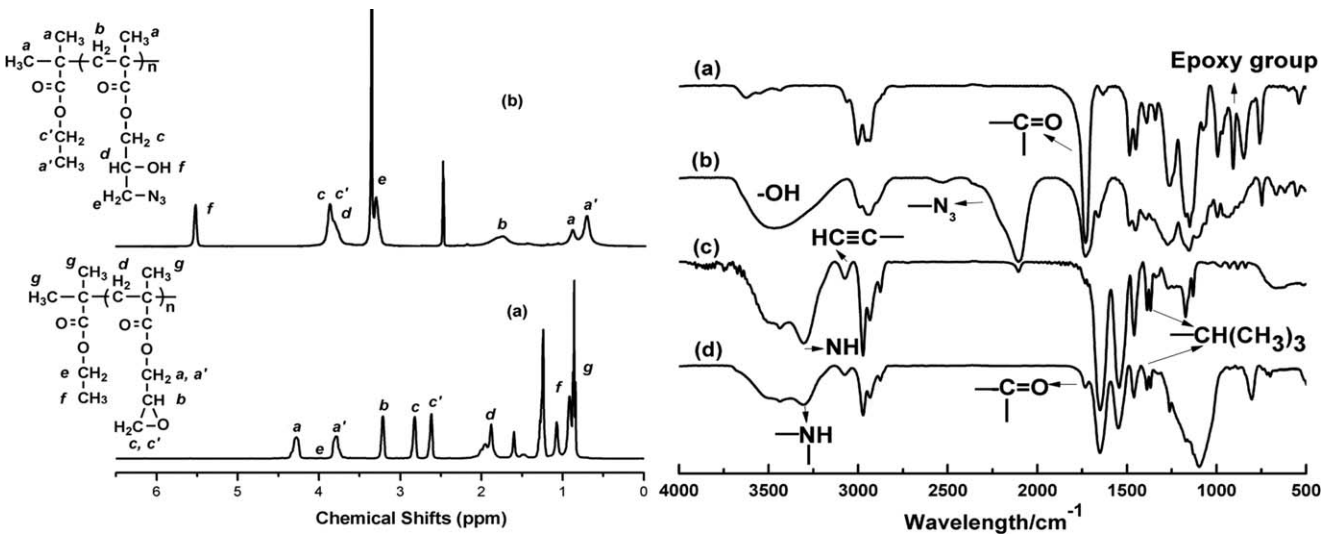

FIGURE 1 ^{1}H NMR spectra (left) for (a) PGMA-Br and (b) PGMA-OH/N_3; FTIR spectra (right) for (a) PGMA-Br, (b) PGMA-OH/N_3, (c) alkynyl-PNIPAM, and (d) PGMA-*g*-PNIPAM.

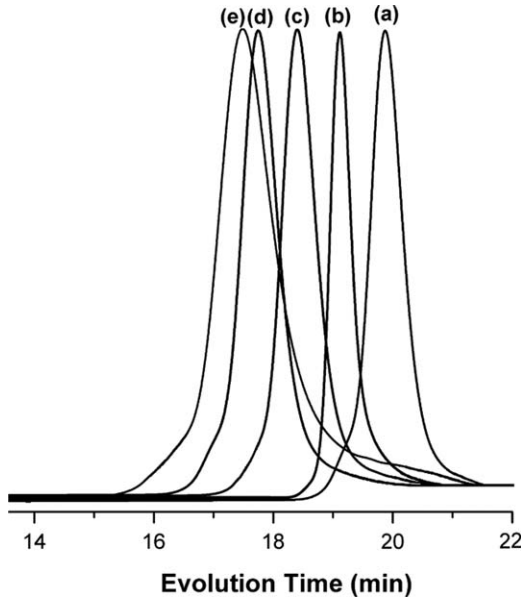

FIGURE 2 GPC curves for (a) alkynyl-PNIPAM$_{20}$, (b) alkynyl-PNIPAM$_{46}$, (c) alkynyl-PNIPAM$_{73}$, (d) PGMA$_{45}$, and (e) PGMA-OH/N$_3$.

confirmed by ^{1}H NMR and FTIR. Compared with its precursor, the signals of epoxy in PGMA at 3.22, 2.83, and 2.62 ppm disappeared completely, and new peaks were observed at 5.50 ppm representing the hydroxyl groups, a broad peak about 3.75–4.08 ppm representing methene protons next to the ester groups, and the methine and methine protons next to the hydroxyl groups [Fig. 1(left b)]. A broad peak at 3670–3200 cm^{-1} for hydroxyl groups is observed in Figure 1(right b), and a new broad band of 2103 cm^{-1} is attributed to the azide group. Meanwhile, the absorbance band of 908 cm^{-1} corresponding to epoxy group disappeared completely. These results all indicated that the epoxy groups on PGMA were successfully hydrolyzed by acid.

Homopolymer PNIPAM with narrow molecular weight distribution was prepared by RAFT polymerization, using *S*−1-butyl-*S*′-(α-methyl-α′-propargyl acetate) trithiocarbonate as RAFT agent characterized systematically and proved to have high purity [Fig. 3(a,c)]. To investigate the influence of the length of the side chain on the thermoresponsive of graft polymers, other two kinds of alkynyl-PNIPAM (DP = 20 and DP = 73) were synthesized and characterized by FTIR, ^{1}H NMR, and ^{13}C NMR. The characteristic peaks were appeared at 3.96 ppm attributing to the methine group next to the amine, at 6–7 ppm corresponding to the hydrogen of secondary amine, and at 2.11 and 1.1–1.3 ppm ascribing to the peaks of hydrogen on the main chain. The peaks of end group were appeared at 4.6 ppm ascribing to methylene protons of propargyl residues [Fig. 3(b)]. Comparing with the ^{13}C NMR spectrum of chain transfer agent, some new peaks were shown at 179.6 ppm for amide group, at 31.6 and 44.3 ppm for the main chain of PNIPAM, and at 23.7 ppm for methyl group [Fig. 3(d)]. For the polymer PNIPAM had large molecular weight and structure, and the end alkyne groups were not very clearly shown because of the low content [Fig. 3(d)]. Meanwhile, the characteristic bands of alkynyl-PNIPAM at 3309 cm^{-1} ascribed to alkynyl group, at 1645 cm^{-1}

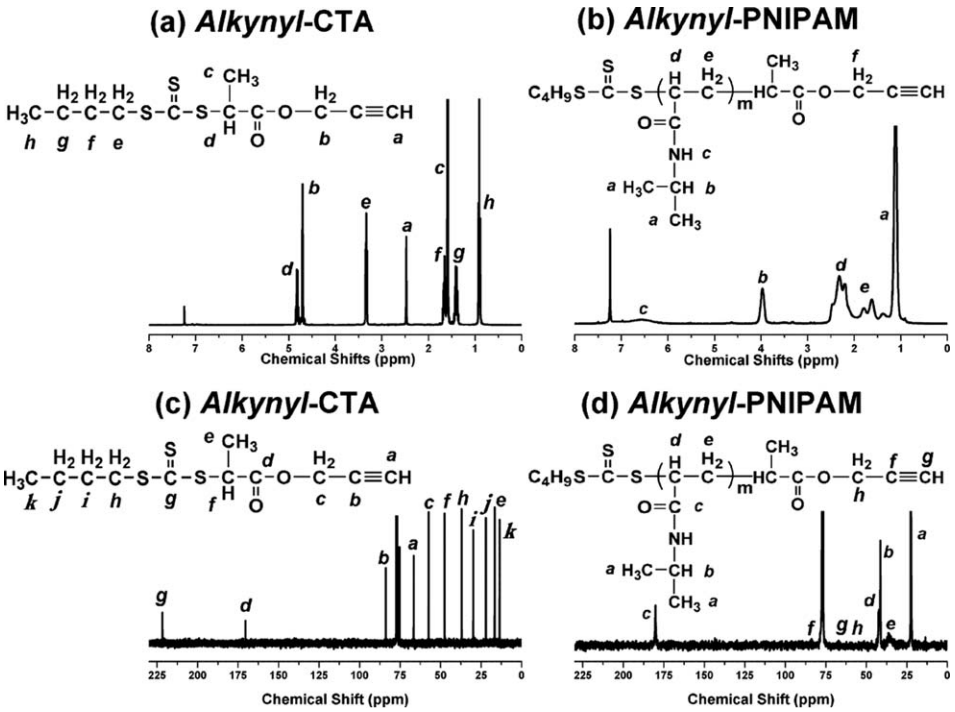

FIGURE 3 ^{1}H NMR spectra and ^{13}C NMR of *S*−1-butyl-*S*′-(α-methyl-α′-propargyl acetate) trithiocarbonate in (a) and (c), alkynyl-PNIPAM in (b) and (d).

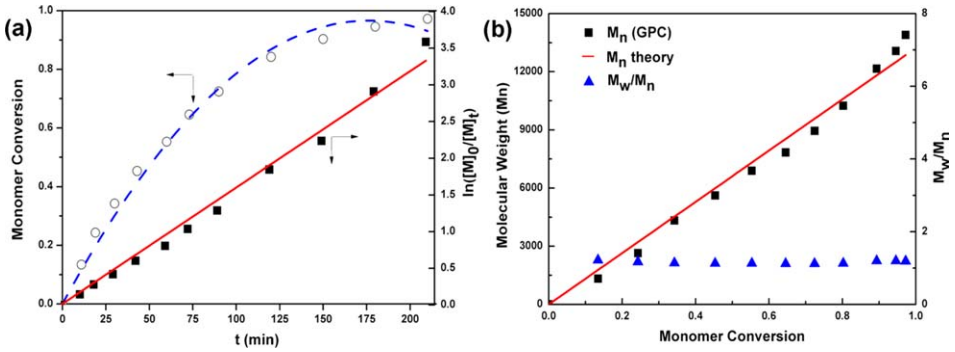

FIGURE 4 Semilogarithmic kinetic plot (a) and the dependence of molecular weight M_n and the molecular weight polydispersity (M_w/M_n) (b) upon the monomer conversion for RAFT of alkynyl-PNIPAM at 70 °C ($[NIPAM]_0/[CTA]_0/[AIBN]_0 = 100:1:0.1$). [Color figure can be viewed in the online issue, which is available at wileyonlinelibrary.com.]

attributed to amide group, and at 1387 and 1366 cm^{-1} attributed to isopropyl group are clearly observed in Figure 1(right c). Only a unimodal and symmetric peaks with narrow molecular distribution for alkynyl-PNIPAMs containing different DPs are found in GPC curves shown in Figure 2(a–c) after RAFT polymerization. All these evidences proved the successful synthesis of alkynyl-PNIPAM.

To better understand the living/controlled character of RAFT polymerization using RAFT agent with alkyne as the end group, the polymerization kinetic of chain growth experiment for alkynyl-PNIPAM was investigated by ^{1}H NMR and GPC. On the basis of the results of ^{1}H NMR and GPC, the relationship of monomer conversion and $\ln([M]_o/[M]_t)$ with polymerization time was conducted at $[NIPAM]_0/[CTA]_0/[AIBN]_0 = 100:1:0.1$. It could be seen from the semilogarithmic kinetic plot in Figure 4 that the monomer conversion increased with the time and reached a high value (>90%) after 2.5 h. As shown in Figure 4(a), $\ln([M]_o/[M]_t)$ was proportional to the polymerization time and showed a linear relationship under the experimental conditions. This revealed that the copolymerization rate was proportional to the monomer conversion and the concentration of growing radicals remained constant during the polymerization and no detectable termination occurred during the polymerization. It proved that the RAFT agent had enough chain transfer capability to promote the homopolymerization reaction even though bearing alkyne group in the structure. The GPC traces of relationship between the number molecular weight and polydispersity versus monomer conversion for RAFT are depicted in Figure 4(b). The straight line in the plot referred to the theoretical molecular weight at a certain monomer conversion. A linear increase of the molecular weight with monomer conversion was observed, and the measured values of M_n were close to the theoretical prediction. Besides, the molecular weight distributions of all samples were narrow (PDIs < 1.35) within the investigated conversion range.

In this research, we used PGMA-OH/N_3 and alkynyl-PNIPAM with different DPs as the reactive materials to prepare graft

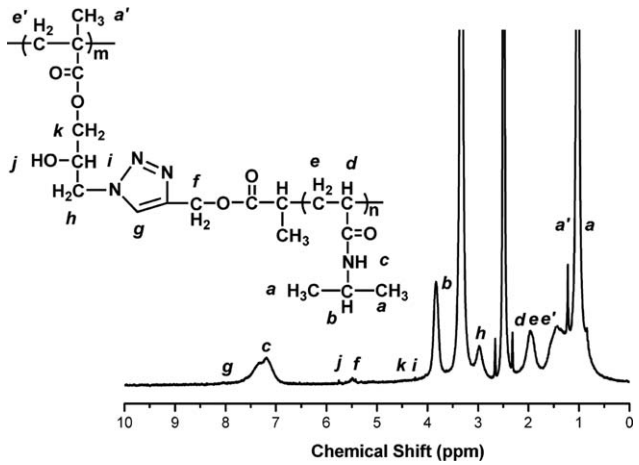

FIGURE 5 ^{1}H NMR spectrum for PGMA-*g*-PNIPAM.

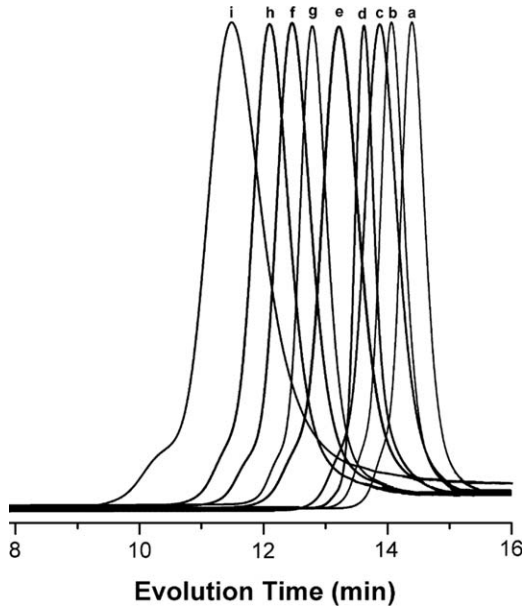

FIGURE 6 GPC curves of $PGMA_{45}$-*g*-$PNIPAM_x$ with different DP and graft efficiency of PNIPAM: (a) DP = 20, 25%, (b) DP = 20, 50%, (c) DP = 20, 75%, (d) DP = 46, 25%, (e) DP = 46, 50%, (f) DP = 46, 75%, (g) DP = 73, 25%, (h) DP = 73, 50%, and (i) DP = 73, 75%.

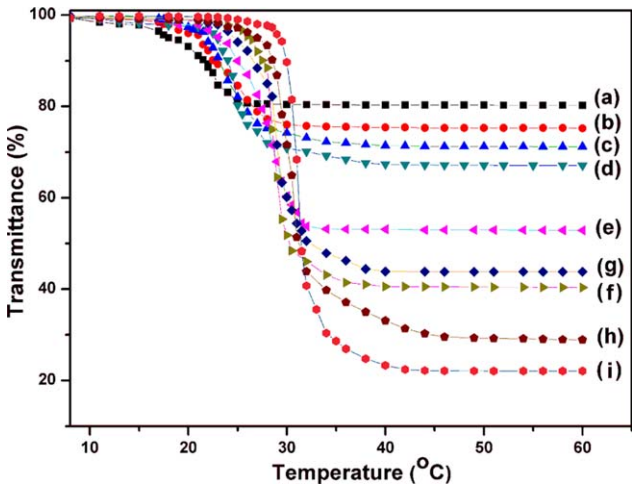

FIGURE 7 Transmittance changes of $PGMA_{45}$-*g*-$PNIPAM_x$ [(a) DP = 20, 25%, (b) DP = 20, 50%, (c) DP = 20, 75%, (d) DP = 46, 25%, (e) DP = 46, 50%, (f) DP = 46, 75%, (g) DP = 73, 25%, (h) DP = 73, 50%, and (i) DP = 73, 75%] aqueous solutions with temperature. [Color figure can be viewed in the online issue, which is available at wileyonlinelibrary.com.]

polymers with different length and graft density of side chains by click chemistry. All graft polymers were systematically characterized by ^{1}H NMR and FTIR. As we could see from ^{1}H NMR, the new resonance peak at 8.2 ppm was observed after click cyclization, which was ascribed to the proton of triazole ring. When compared with that of alkynyl-PNIPAM, the peak at 4.6 ppm completely shifted to 5.3 ppm and a new peak at 5.5 ppm ascribed to hydroxyl group in the side chain of PGMA was appeared (Fig. 5). From the FTIR curve of Figure 1(right d), we could observe the disappearance of characteristic azide absorbance peak at 2105 cm^{-1} for PGMA-OH/N_3 and a broad absorbance peak at 1590–1800 cm^{-1} mixed with the amide and carbonyl group was appeared when compared with that of alkynyl-PNIPAM. Moreover, the relative intensity of the absorbance peak at 3302 cm^{-1}, attributed to the characteristic band of —NH—, also decreased considerably. It was worthy of noting that GPC traces of graft polymers (PGMA-*g*-PNIPAM) were nearly monomodal and symmetric; this and a clear shift of the elution peak toward the higher molecular weight was observed with a weak shoulder peak, which was caused by the huge hindrance and high density for the huge molecular structure (Fig. 6). Thus, all these results suggested successful cyclization via the "click" mechanism.

The graft polymers containing PNIPAM with different graft length and graft density underwent a clear phase separation when the temperature was higher than the LCST. The effect of changing the temperature of PGMA-*g*-PNIPAM aggregates in aqueous solution on the transmittance was studied by UV–vis spectroscopy, and the cloud point curves showed a plot of the transmittance versus temperature.

When the length of the main chain was kept the same, the LCST values of the graft polymers exhibited a correlation between the graft density and the grafting length as well as the molecular weight. As we could know from Figure 7 that with longer graft length and larger density of side chain, the content of the hydrophilic portion of the graft polymers was higher and the interaction forces between polymer and water were stronger and more extensive, leading to a bigger LCST value that was closer to that of PNIPAM. Figure 7 also illustrates that the longer length of PNIPAMs had the temperatures at 90% transmittance for these macromolecular aqueous solutions were higher, which were closer to that of linear PNIPAM solution, while the values of LCST for these micelle solutions were broader and lower than that of PNIPAM. We also found that bearing the same length of main chain and side chain, but the macromolecular aqueous solutions with different graft densities of the side chains, being denser graft densities had the bigger temperature values of 90% transmittance, which was closer to the property of PNIPAM. The tendency was similar with the same graft density and different length of PNIPAM. Although polymer g ($PGMA_{45}$-*g*-$PNIPAM_{(73,\ 25\%)}$) had a longer graft length than that of polymer f ($PGMA_{45}$-*g*-$PNIPAM_{(46,\ 75\%)}$), its LCST value was smaller according to the curves. This may be ascribed to the balance of forces between polymer–water and polymer–polymer interactions in the aqueous solutions.[50] It could be known that when the length of the main chain was the same, the graft polymer g with longer PNIPAM made it difficult for water molecules to contact with the PNIPAM, thus presented a lower LCST value because of weaker interactions of PNIPAM–water. Meanwhile, polymers with shorter length and lower graft density of PNIPAM had lower values of transmittance and LCST, and were easy to keep the transmittance value constant. These may be related with the structures of these graft polymers. The backbones of graft polymers were hard to touch with the water molecules, increasing PNIPAM side-chain lengths and graft densities lead to strengthen the hydrophilic property of the macromolecular brushes and the LCST values of graft polymers. These results were in good accordance with that of Zhao group, which also suggested that the macromolecules with long side chain and graft density of PNIPAM had the bigger LCST value.[49] In our research, even when the PNIPAM side chains were densely grafted onto the main chain, the LCST values were appeared and closer to that of the linear polymer PNIPAM. What's more, when the length of side chain and graft density of polymers became lower and lower, such as a and b, the saturation platforms of transmittance were weak and even kept constant, which was also concluded from the reference.[51] This results indicated that the length and the graft density had positive co-relationship with the phase separation behavior and LCST change.

We also conducted further study to investigate the effect of changing the temperature of the PGMA-*g*-PNIPAM aggregates in aqueous solution on the diameters of the graft polymers by DLS. Graft polymer (9.0 mg) was dissolved in 0.8 mL THF and vigorously stirred for 24 h, then 6 mL cold twice-distilled water was slowly added into the mixture and stirred for 2 days. After removing THF by dialysis bag, the

TABLE 2 Size Distributions of Amphiphilic Polymers in Aqueous Solution at 18 and 40 °C[a]

	18 °C		40 °C	
Sample	Diameter (nm)[b]	PDI	Diameter (nm)[b]	PDI
$PGMA_{45}$-*g*-$PNIPAM_{20,\ 25\%}$	101.1	0.112	85.1	0.126
$PGMA_{45}$-*g*-$PNIPAM_{20,\ 50\%}$	112.7	0.125	96.4	0.145
$PGMA_{45}$-*g*-$PNIPAM_{20,\ 75\%}$	132.3	0.126	117.5	0.148
$PGMA_{45}$-*g*-$PNIPAM_{46,\ 25\%}$	152.1	0.122	124.2	0.153
$PGMA_{45}$-*g*-$PNIPAM_{46,\ 50\%}$	193.3	0.132	161.3	0.165
$PGMA_{45}$-*g*-$PNIPAM_{46,\ 75\%}$	247.3	0.141	174.3	0.171
$PGMA_{45}$-*g*-$PNIPAM_{73,\ 25\%}$	238.4	0.142	169.8	0.168
$PGMA_{45}$-*g*-$PNIPAM_{73,\ 50\%}$	302.5	0.151	205.4	0.188
$PGMA_{45}$-*g*-$PNIPAM_{73,\ 75\%}$	352.8	0.168	251.7	0.195

[a] Conditions: 0.3 wt %.

[b] Number-average mean diameter by DLS.

micelle solution was used to measure the diameter and particle dispersion index (PDI) by DLS at 18 and 40 °C, respectively. The diameter and PDI of aggregates in aqueous solution are shown in Table 2. It could be concluded that graft polymers with longer and denser graft density of PNIPAM side chain had larger diameter in 18 °C and with increasing the temperature above 40 °C, the diameters of all polymers decreased compared to those at 18 °C.

These results could be explained as follows and the relative schematic illustration is shown in Figure 8: the solutions of graft polymers could be self-assemble to micelles with PGMA as core and PNIPAM side chains as shell when the temperature was below the LCST, so polymers with longer and denser graft density of PNIPAM side chain having bigger molecular weight were liable to form larger aggregates. The samples, such as $PGMA_{45}$-*g*-$PNIPAM_{(73,\ 50\%)}$ and $PGMA_{45}$-*g*-$PNIPAM_{(73,\ 75\%)}$, had bigger diameter at different temperatures than others, while the reduced rates at 40 °C of them were faster than other systems. This may be ascribed to the stronger repulsion of denser PNIPAM side chains, which lead to decreasing the radius of curvature of the micelle aggregates. When the temperature was above LCST, the full stretching hydrophilic side chains PNIPAM in aqueous dehydrated and then collapsed to form hydrophobic segments. Therefore, these shrinking structures decreased the stability

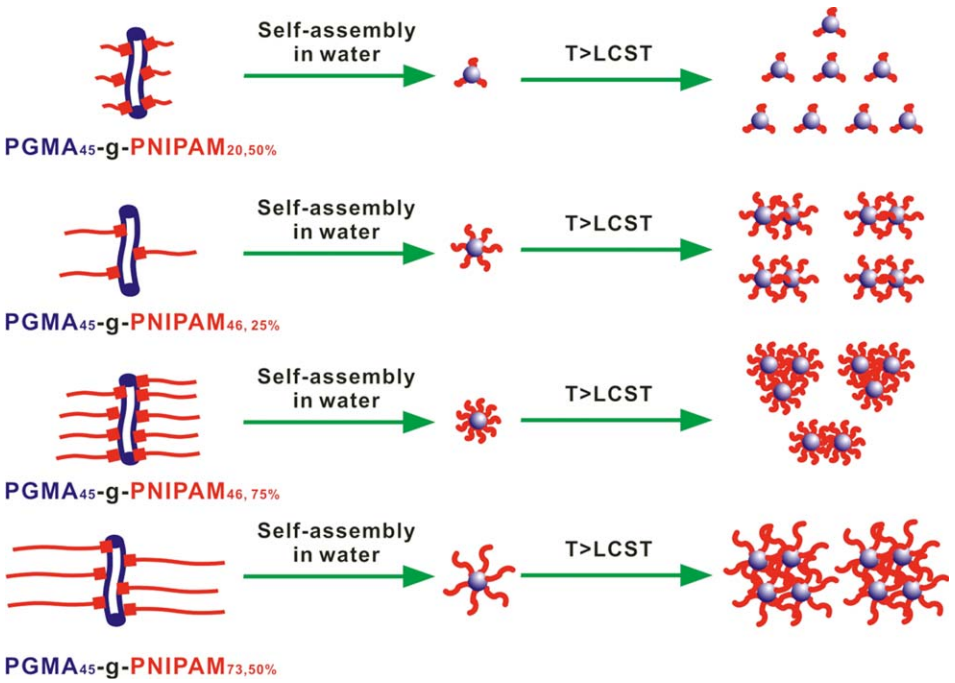

FIGURE 8 Schematic illustration of aggregation behavior for the graft polymers at different temperatures. [Color figure can be viewed in the online issue, which is available at wileyonlinelibrary.com.]

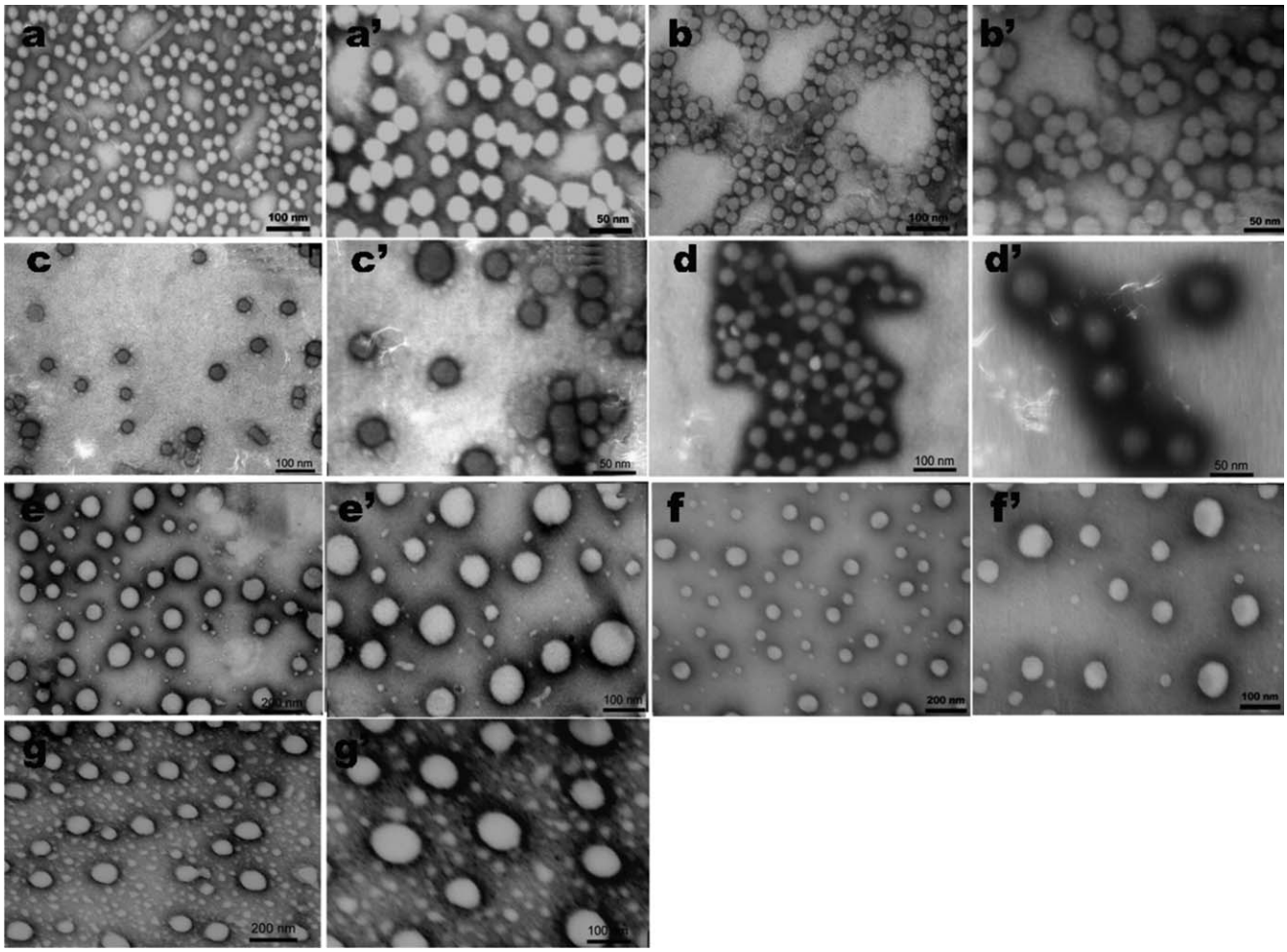

FIGURE 9 TEM images and their high-magnification images of graft polymer solutions (a, a′) $PGMA_{45}$-*g*-$PNIPAM_{(20,\ 50\%)}$, (b, b′) $PGMA_{45}$-*g*-$PNIPAM_{(20,\ 75\%)}$, (c, c′) $PGMA_{45}$-*g*-$PNIPAM_{(46,\ 25\%)}$, (d, d′) $PGMA_{45}$-*g*-$PNIPAM_{(46,\ 50\%)}$, (e, e′) $PGMA_{45}$-*g*-$PNIPAM_{(46,\ 75\%)}$, (f, f′) $PGMA_{45}$-*g*-$PNIPAM_{(73,\ 25\%)}$, and (g, g′) $PGMA_{45}$-*g*-$PNIPAM_{(73,\ 50\%)}$ at room temperature.

of the micelle and also reduced the diameter, which could be seen from the changes of Table 2. This result agreed quite well with Huang's report, indicating that higher graft density would form irregular morphology and make the size distribution asymmetric because of steric hindrance between graft side chains.[9] Paris and Garrido also found that the molecular weight and PDI had a notable effect on the diameter and size distribution of the formed micelles.[52]

It has been studied that the aggregation morphology of polymer micelle was depended on three main parameters: the stretching of the core, interfacial tension between the core and the solvent, and the intercorona repulsion, and the morphology could be changed by adjusting the balance of these three forces. In this article, we chose a series of graft polymer micelles to investigate the effect of the graft length and the content of the graft density on the self-assembly morphology. The micelle morphologies of seven thermoresponsive graft polymers were observed by TEM, and Figure 9(a–g) shows the relative TEM images and high-magnification images of micelles for $PGMA_{45}$-*g*-$PNIPAM_{(20,\ 50\%)}$, $PGMA_{45}$-*g*-$PNIPAM_{(20,\ 75\%)}$, $PGMA_{45}$-*g*-$PNIPAM_{(46,\ 25\%)}$, $PGMA_{45}$-*g*-$PNIPAM_{(46,\ 50\%)}$, $PGMA_{45}$-*g*-$PNIPAM_{(46,\ 75\%)}$, $PGMA_{45}$-*g*-$PNIPAM_{(73,\ 25\%)}$, and $PGMA_{45}$-*g*-$PNIPAM_{(73,\ 50\%)}$ at room temperature. Some similar spherical-shaped microspheres were embedded in the stable micelles for a and a′ with the diameter range of 24–32 nm, b and b′ of 26–36 nm, c and c′ of 29–36 nm, d and d′ of 33–40 nm, e and e′ of 65–95 nm, and f and f′ of 53–88 nm. It could be explained that the main-chain PGMA as backbone is hard to be soluble in the water and then curls up to be random coils during the self-assembly process, while the hydrophilic moiety can be miscible with water and then stretches on the outside. This morphology is closely related with the different solubility of the structure, and the schematic diagram for the self-assembly of the block copolymer into micelle structure is shown in Figure 8. For the spherical-like morphology of graft polymer $PGMA_{45}$-*g*-$PNIPAM_{(73,\ 50\%)}$ with longer graft length and higher graft efficiency, shown in g and g′, was observed by TEM. This morphology was closely related with the architecture of the side chain for polymer $PGMA_{45}$-*g*-$PNIPAM_{(73,\ 50\%)}$, and some small nanoparticles were embedded in the system,

which may be the small aggregates in the micelles. We could conclude from the TEM observation that the graft length and density had a significant effect on the mean diameter of micelle, but they had no obvious effect on the self-assembly morphology, which was satisfied with the characteristic of the star-like micelle.

CONCLUSIONS

In this article, we successfully designed and prepared a series of thermoresponsive graft polymers composed of poly(glycidyl methacrylate) (PGMA) as backbone and PNIPAM as side chain with different length and graft density by a combination of atom transfer radical polymerization (ATRP), reversible addition-fragmentation chain transfer (RAFT) polymerization, and click chemistry. The process included: synthesis of homopolymer PGMA via ATRP and then ring-opening the pendent oxirane groups, preparation of alkynyl-terminated PNIPAM by RAFT polymerization, and finally click reaction of two linear homopolymers in the presence of CuBr/PMDETA. These different graft polymers were used to investigate the effect of the graft length and graft density on the thermoresponsive behavior and self-assemble morphology. The thermoresponsive property was measured by UV–vis spectroscopy and DLS, which proved that the length and graft density as well as the molecular weights had positive co-relationship with the LCST value and diameter of micelles as well as the size distribution. The graft polymers with larger molecular weight and density of side chains had higher LCST values, and the aggregates also had bigger mean diameter though they had strong steric repulsive interactions with each other. The self-assembly behaviors of graft polymers in aqueous solution showed that nanoscopic microspheres were embedded in the stable micelles of $PGMA_{45}$-*g*-$PNIPAM_{25}$ and $PGMA_{45}$-*g*-$PNIPAM_{46}$ with the increase of the diameters, while the main morphology of $PGMA_{45}$-*g*-$PNIPAM_{(75,\ 50\%)}$ aqueous solution with longer length and graft density was spherical-like nanoparticles with two kinds of particle size distribution, which indicated that the graft length and density on the side chain for the graft polymer had more significant effect on the diameter than the self-assemble morphology. There results could give some valuable guidance for designing and fabricating some functional polymers, and also provide some important information for investigating the relationship between the architecture and the functional properties.

ACKNOWLEDGMENTS

This work was supported by the integration of Industry, Education and Research of Guangdong Province Project (2011A091000007), and Foshan and Chinese Academy of Sciences Cooperation project (2011BY100341).

REFERENCES AND NOTES

1 S. E. Stiriba, H. Kautz, H. Frey, *J. Am. Chem. Soc.* **2002**, *124*, 9698–9699.

2 J. Rodriguez-Hernandez, S. Lecommandoux, *J. Am. Chem. Soc.* **2005**, *127*, 2026–2027.

3 D. Neugebauer, *Polymer* **2007**, *48*, 4966–4973.

4 X. H. Zhang, Z. Shen, C. Feng, D. Yang, Y. G. Li, J. H. Hu, G. L. Lu, X. Y. Huang, *Macromolecules* **2009**, *42*, 4249–4256.

5 Y. Deng, S. Zhang, G. L. Lu, X. Y. Huang, *Polym. Chem.* **2013**, *4*, 1289–1299.

6 N. V. Tsarevsky, S. A. Bencherif, K. Matyjaszewski, *Macromolecules* **2007**, *40*, 4439–4445.

7 J. P. Sun, J. W. Hu, G. J. Liu, D. S. Xiao, G. P. He, R. F. Lu, *J. Polym. Sci. Part A: Polym. Chem.* **2011**, *49*, 1282–1288.

8 D. Neugebauer, Y. Zhang, T. Pakula, K. Matyjaszewski, *Polymer* **2003**, *44*, 6863–6871.

9 X. S. Fan, G. W. Wang, Z. Zhang, J. L. Huang, *J. Polym. Sci. Part A: Polym. Chem.* **2011**, *49*, 4146–4153.

10 N. Hadjichristidis, H. Iatrou, M. Pitsikalis, J. Mays, *Prog. Polym. Sci.* **2006**, *31*, 1068–1132.

11 P. P. Li, Z. Y. Li, J. L. Huang, *Polymer* **2007**, *48*, 1557–1566.

12 (a) M. F. Zhang, T. Breiner, H. Mori, A. H. E. Muller, *Polymer* **2003**, *44*, 1449–1458; (b) C. Cheng, K. Qi, E. Khoshdel, K. L. Wooley, *J. Am. Chem. Soc.* **2006**, *128*, 6808–6809; (c) C. Liang, J. Q. Liu, R. Wang, Z. Liu, W. R. Yang, *J. Polym. Sci. Part A: Polym. Chem.* **2012**, *50*, 4423–4432.

13 (a) M. Schappacher, A. Deffieux, *Science* **2008**, *319*, 1512–1515; (b) Q. Fu, W. C. Lin, J. L. Huang, *Macromolecules* **2008**, *41*, 2381–2387.

14 (a) M. Elsabahy, K. L. Wooley, *J. Polym. Sci. Part A: Polym. Chem.* **2012**, *56*, 1869–1880; (b) L. Zhou, K. Zhang, J. Ma, C. Cheng, K. L. Wooley, *J. Polym. Sci. Part A: Polym. Chem.* **2009**, *47*, 5557–5563; (c) S. S. Sheiko, B. S. Sumerlin, K. Matyjaszewski, *Prog. Polym. Sci.* **2008**, *33*, 759–785.

15 G. Riess, *Prog. Polym. Sci.* **2003**, *28*, 1107–1170.

16 Y. Cai, Y. Tang, S. P. Armes, *Macromolecules* **2004**, *37*, 9728–9737.

17 C. G. Sabchez, D. Wouters, C. A. Fustin, J. F. Gohy, B. G. G. Lohmeijer, U. S. Schubert, *Macromolecules* **2005**, *38*, 10185–10191.

18 Y. Q. Zhang, Z. Shen, D. Yang, C. Feng, J. H. Hu, G. L. Lu, X. Y. Huang, *Macromolecules* **2010**, *43*, 117–125.

19 Y. G. Li, Y. Q. Zhang, D. Yang, Y. J. Li, J. H. Hu, C. Feng, S. J. Zhai, G. L. Lu, X. Y. Huang, *Macromolecules* **2010**, *43*, 262–270.

20 Y. R. Ren, X. S. Jiang, J. Yin, *Eur. Polym. J.* **2008**, *44*, 4108–4114.

21 Y. Y. Zhang, H. Liu, J. M. Hu, C. H. Li, S. Y. Liu, *Macromol. Rapid Commun.* **2009**, *30*, 941–947.

22 C. Weber, C. R. Becer, W. Guenther, R. Hoogenboom, U. S. Schubert, *Macromolecules* **2010**, *43*, 160–167.

23 W. Zhang, X. Zhou, H. Li, Y. Fang, G. Zhang, *Macromolecules* **2005**, *38*, 909–914.

24 M. Yamato, C. Konno, M. Utsumi, A. Kikuchi, T. Pkano, *Biomaterials* **2002**, *23*, 561–567.

25 H. Suzuki, H. M. Nurul, T. S. Kawamoto, H. Haga, K. Kawabata, Y. Takeoka, *Macromolecules* **2010**, *43*, 9945–9956.

26 N. M. L. Hansen, K. Jankova, S. Hvilsted, *Eur. Polym. J.* **2007**, *43*, 255–293.

27 V. Sciannamea, R. Jrme, C. Detrembleur, *Chem. Rev.* **2008**, *10*, 1104–1126.

28 H. F. Gao, K. Matyjaszewski, *Prog. Polym. Sci.* **2009**, *34*, 317–350.

29 K. Matyjaszewski, J. H. Xia, *Chem. Rev.* **2001**, *101*, 2921–2990.

30 M. Ouchi, T. Terashima, M. Sawamoto, *Chem. Rev.* **2009**, *109*, 4963–5124.

31 C. B. Kowollik, S. Perriert, *J. Polym. Sci. Part A: Polym. Chem.* **2008**, *46*, 5715–5723.

32 G. Moad, E. Rizzardo, S. H. Thang, *Polymer* **2008**, *49*, 1079–1131.

33 G. Moad, E. Rizzardo, S. H. Thang, *Aust. J. Chem.* **2012**, *65*, 985–1076.

34 H. W. Chen, J. F. Li, Y. W. Ding, G. Z. Zhang, *Macromolecules* **2005**, *38*, 4403–4408.

35 D. C. Li, Y. Cui, K. W. Wang, Q. He, X. H. Yan, J. B. Li, *Adv. Funct. Mater.* **2007**, *17*, 3134–3140.

36 W. H. Chiang, Y. H. Hsu, Y. W. Chen, C. S. Chern, H. C. Chiu, *Macromol. Chem. Phys.* **2011**, *212*, 1869–1878.

37 T. Cai, M. Li, K. G. Neoh, E. T. Kang, *J. Mater. Chem.* **2012**, *22*, 16248–16258.

38 H. C. Kolb, M. G. Finn, K. B. Sharpless, *Angew. Chem. Int. Ed.* **2001**, *40*, 2004–2021.

39 A. Gregory, M. H. Stenzel, *Prog. Polym. Sci.* **2012**, *37*, 38–105.

40 R. Fu, G. D. Fu, *Polym. Chem.* **2011**, *2*, 465–475.

41 Z. P. Cheng, X. L. Zhu, E. T. Kang, K. G. Neoh, *Langmuir* **2005**, *21*, 7180–7185.

42 C. H. Li, Z. S. Ge, J. Fang, S. Y. Liu, *Macromolecules* **2009**, *42*, 2916–2924.

43 K. Huang, J. Rzayev, *J. Am. Chem. Soc.* **2009**, *131*, 6880–6885.

44 Z. P. Cheng, X. L. Zhu, G. D. Fu, E. T. Kang, K. G. Neoh, *Macromolecules* **2005**, *38*, 7187–7192.

45 X. M. Lian, D. X. Wu, X. H. Song, H. Y. Zhao, *Macromolecules* **2010**, *43*, 7434–7445.

46 C. Z. Zhao, D. X. Wu, X. M. Lian, Y. Zhang, X. H. Song, H. Y. Zhao, *J. Phys. Chem. B* **2010**, *114*, 6300–6308.

47 T. Cai, K. G. Neoh, E. T. Kang, *Langmuir* **2011**, *27*, 2936–2945.

48 G. D. Fu, L. Q. Xu, F. Yao, K. Zhang, X. F. Wang, M. F. Zhu, S. Z. Nie, *Appl. Mater. Int.* **2009**, *1*, 239–243.

49 D. X. Wu, X. H. Song, T. Tang, H. Y. Zhao, *J. Polym. Sci. Part A: Polym. Chem.* **2010**, *48*, 443–453.

50 H. G. Schild, *Prog. Polym. Sci.* **1992**, *17*, 163–249.

51 Z. L. Liu, J. W. Hu, J. P. Sun, G. P. He, Y. H. Li, G. W. Zhang, *J. Polym. Sci. Part A: Polym. Chem.* **2010**, *48*, 3573–3586.

52 R. Paris, I. Q. Garrido, *J. Polym. Sci. Part A: Polym. Chem.* **2011**, *49*, 1928–1932.